

SU(3) deconfining phase transition with finite volume corrections due to a confined exterior

Bernd A. Berg and Hao Wu

Department of Physics, Florida State University, Tallahassee, FL 32306-4350

(December 3, 2024)

Using the geometry of a double-layered torus we investigate the deconfining phase transition of pure SU(3) lattice gauge theory by Markov chain Monte Carlo simulations. In one layer, called “outside”, the temperature is set below the deconfining temperature and in the other, called “inside”, it is iterated to a pseudo-transition temperature. Lattice sizes are chosen in a range suggested by the physical volumes achieved in relativistic heavy ion collisions and both temperatures are kept close enough to stay in the SU(3) scaling region. Properties of the transition are studied as function of the volume for three outside temperatures. When compared with infinite volume extrapolations, small volume corrections of the deconfining temperature and width become competitive with those found by including quarks. Effective finite size scaling exponents of the specific and Polyakov loop susceptibilities are also calculated.

PACS: 11.15.Ha, 12.38.Mh, 25.75.Nq, 64.60.an

I. INTRODUCTION

Experimentally the deconfining phase transition has been studied in heavy ion scattering experiments, notably at the Relativistic Heavy Ion Collider (RHIC) of Brookhaven National Lab and at the LHC at CERN. Markov chain Monte Carlo (MCMC) simulations of lattice gauge theory (LGT) provide theoretical estimates for thermodynamic quantities of this phase transition, in particular for the temperature and width. Inevitably a quark-gluon plasma phase created in a laboratory experiment is limited to a small hot volume, which is surrounded by a cold exterior. In contrast to the physical situation of heavy ion collisions, most of the theoretical work on the deconfining phase transitions focused on the infinite volume limit in which boundary effects become negligible. Notable exceptions are provided by some older work [1] and more recent investigations of finite volume effects for pure SU(3) lattice gauge theory [2,3], for QCD [4–6] and for a Polyakov-Nambu-Jona-Lasinio model [7].

Building on [2,3], the aim of our simulations of this paper is to investigate for pure SU(3) lattice gauge theory effects due to relatively small temperature at the boundaries, so that both volumes can be kept in the SU(3) scaling region. We use the Wilson action [8] on a 4D hypercubic lattice. Lattice configurations are weighted with a Boltzmann factor $\exp[S(\{U\})]$, where

$$S(\{U\}) = \sum_{\square} \beta_{\square} S_{\square}, \quad (1)$$

$$S_{\square} = \frac{1}{3} \operatorname{Re} (U_{i_1 j_1} U_{j_1 i_2} U_{i_2 j_2} U_{j_2 i_1}).$$

Here i_1, j_1, i_2 and j_2 label the sites circulating about the square \square and the U_{ij} are SU(3) matrices. For later convenience we allow the coupling constant

$$g_{\square}^2 = 6/\beta_{\square} \quad (2)$$

to depend on the position of the plaquette.

We set the scale in our calculations by choosing the transition temperature in the infinite volume extrapolation to be

$$T_t = 174 \text{ MeV}. \quad (3)$$

This temperature is in the bulk of LGT estimates of the deconfining temperature with quarks included. See [9] for a recent overview. Often the physical scale in pure gauge calculations is set by choosing a value of $\sqrt{\sigma} \approx 420 \text{ MeV}$ for the string tension σ . Via scaling one finds the ratio $T_t/\sqrt{\sigma} = 0.629(3)$ for the SU(3) continuum limit [10], so that in this approximation $T_t \approx 260 \text{ MeV}$. We see that the corrections due to quarks amount to about 1/3 of this value. In the present paper we are interested in finite volume corrections to the QCD estimate of T_t . Therefore, we do not set the scale by the string tension but by the transition temperature at its QCD value (3), which we convert into the lambda scale (27), using finally $\Lambda_L = 5.07 \text{ MeV}$ (28) to express physical quantities in units of MeV.

Most LGT calculations use periodic boundary conditions (PBC), because they ensure a fast approach of the infinite volume limit. But they are not suitable when one wants to study the effect of an exterior confined phase on a small volume, which is either deconfined or at the transition temperature. In previous work [2] zero outside temperature was targeted and modeled by the strong coupling limit $a(\beta) \rightarrow \infty$ for $\beta \rightarrow 0$, called cold boundary condition (CBC). For realistically sized volumes corrections to the transition temperature (3) were found in a range from 30 MeV down to 10 MeV when compared to signals of the deconfinement transition relevant for large volumes. Although agreement with SU(3) scaling was seen when varying the temporal lattice extension N_{τ} from 4 to 6, one has to be worried because the construction mixes a SU(3) scaling region with BCs defined by the strong coupling limit.

To make sure that the encountered corrections are not a strong coupling artifact, we consider in the present article differences between inside and outside temperature that are small enough so that both regions can be kept in the SU(3) scaling region. Outside temperatures are taken close to

$$T_1 = 158 \text{ MeV}, T_2 = 162 \text{ MeV} \text{ and } T_3 = 168 \text{ MeV}, \quad (4)$$

while inside temperatures are iterated to pseudo-transition values, which we locate by maxima of the SU(3) Polyakov loop susceptibility. A possible geometry would use for the inside a $N_\tau n_s^3$ sublattice of a $N_\tau N_s^3$ lattice with PBC ($n_s < N_s$). We decided instead to explore the interesting geometry of a double-layered torus (DLT), which joins two $N_\tau N_s^3$ lattices so that each N_s^3 volume provides the boundary of the other [3].

In the next section we give details of the DLT construction. For subsequent reference we present in section III results from simulations on lattices with PBC after introducing our observables and reviewing the status of SU(3) scaling. Using the DLT geometry finite volume correction to the SU(3) deconfining transition are studied in section IV. Off from our main focus, we add in section V a discussion of the finite size scaling exponents of our Polyakov loop susceptibilities for large spatial lattices. Summary and conclusions follow in the final section VI. All MCMC simulations for this paper were performed with the SU(3) Fortran programs which we documented in Ref. [11].

II. DOUBLE-LAYERED TORUS

The DLT [3] extends PBC by using two layers. Let us first recall the definition of PBC for a lattice of size $\prod_{i=1}^4 N_i$. We label its sites by integer 4-vectors

$$n = (n_1, n_2, n_3, n_4)$$

with coordinates $n_i = 0, \dots, N_i - 1$ ($i = 1, \dots, 4$). Steps in forward direction are defined by

$$n_i \oplus 1 = \begin{cases} n_i + 1 & \text{for } n_i < N_i - 1, \\ 0 & \text{for } n_i = N_i - 1, \end{cases} \quad (5)$$

and steps in backward direction by

$$n_i \ominus 1 = \begin{cases} n_i - 1 & \text{for } n_i > 0, \\ N_i - 1 & \text{for } n_i = 0. \end{cases} \quad (6)$$

Our DLT is defined by two identical lattices of size $N_\tau N_s^3$. We label their coordinates by n_i^ℓ , $\ell = 0, 1$. PBC are used in the temporal ($i = 4$) direction. Defining

$$\ell' = \text{mod}(\ell + 1, 2) = \begin{cases} 1 & \text{for } \ell = 0, \\ 0 & \text{for } \ell = 1, \end{cases} \quad (7)$$

the DLT BC in the spacelike directions ($i = 1, 2, 3$) are for steps in forward direction

$$n_i^\ell \oplus 1 = \begin{cases} [n_i + 1]^\ell & \text{for } n_i^\ell < N_i - 1, \\ 0^{\ell'} & \text{for } n_i^\ell = N_i - 1, \end{cases} \quad (8)$$

and for steps in backward direction

$$n_i^\ell \ominus 1 = \begin{cases} [n_i - 1]^\ell & \text{for } n_i^\ell > 0, \\ [N_i - 1]^{\ell'} & \text{for } n_i^\ell = 0. \end{cases} \quad (9)$$

The other layer is entered whenever the same lattice would be entered from the other side in case of PBC. For two spacelike dimensions the topology is that of a Klein bottle.

The usual derivation, for instance [12], of the interpretation of the inverse temporal lattice extension (in which we have PBC) is still valid and we find for equilibrium configurations

$$T = \frac{1}{a(\beta_\ell) N_\tau} \quad (10)$$

for the physical temperature. Here we allow distinct coupling constants β_0 and β_1 for the layers (in LGT β is defined by (2) and not $1/(kT)$). As for the action in Eq. (1) and (2), coupling constants are assigned to entire plaquettes. SU(3) matrices in Eq. (1) are defined on directed links, which originate from sites of the lattice(s) and point forward in one of the four directions (a matrix U is replaced by U^{-1} when it is encountered in reversed direction of the link). Our rule is now that we use the coupling constant value β_1 for a plaquette if any of its links originates in the $\ell = 1$ layer. Otherwise the values β_0 is used. This introduces a slight asymmetry for their assignments in our two layers. The $\ell = 0$ layer will be taken as the outside and the $\ell = 1$ layer as the inside volume.

The MCMC process equilibrates the entire system by providing for each SU(3) matrix the appropriate infinite heatbath reservoir. Distinct couplings in different regions are no obstacle and used as well in other systems like spin glasses. In the infinite volume limit each layer equilibrates at its own temperature and the other layer serves as boundary. At the boundaries a quasi-static region emerges which a temperature gradient from one into the other. For small finite volumes this boundary region may not be negligible.

III. DECONFINING TRANSITION WITH PBC

First we define the observables used in this paper. Subsequently SU(3) scaling and some numerical results with PBC are reviewed. Finally in this section we present our own MCMC simulations with PBC. Each data point relies on 2^{13} sweeps for reaching equilibrium and thereafter 64×2^{13} measurements, each separated from the next by 4 sweeps. Error bars (given in parenthesis) were calculated with respect to jackknife bins so that autocorrelations are properly accounted for. Details about autocorrelations can be found in [19]. Improved estimators relying on the

multi-hit approach [20] were explored, but found rather inefficient in our range of coupling constant values, and the simulations remained very CPU time demanding.

A. Observables

The *specific heat* of the LGT system is

$$C(\beta) = \frac{1}{6N} [\langle S^2 \rangle - \langle S \rangle^2], \quad (11)$$

where N is the total number of lattice sites. Writing the sum over all Polyakov loops on the lattice as

$$P = \sum_{\vec{x}} P_{\vec{x}}, \quad (12)$$

the *magnetic Polyakov loop susceptibility* is defined by

$$\chi = \frac{1}{N_{\vec{x}}} [\langle |P|^2 \rangle - \langle |P| \rangle^2], \quad (13)$$

and the *thermal Polyakov loop susceptibility* by

$$\chi^\beta = \frac{1}{N_{\vec{x}}} \frac{d}{d\beta} \langle |P|^2 \rangle, \quad (14)$$

where $N_{\vec{x}}$ is the total number of spatial lattice sites. As signal for the pseudo-transition temperature we use in this paper the locations of the maxima of the magnetic Polyakov loop susceptibility and drop the adverb “magnetic”. The thermal Polyakov loop susceptibility gives, slightly shifted, similarly strong signals, whereas the maxima of the specific heat are less pronounced.

Another interesting quantity is the *structure factor* (see, e.g., Ref. [13,14])

$$F(\vec{k}) = \frac{1}{N_{\vec{x}}} \left\langle \left| \sum_{\vec{x}} P_{\vec{x}} \exp(i\vec{k}\vec{x}) \right|^2 \right\rangle, \quad \vec{k} = \frac{2\pi}{N_s} \vec{n}, \quad (15)$$

where \vec{n} is an integer vector, which is for our measurements restricted to $(0, 0, 1)$. These quantities are important in the determination of finite size scaling exponents. Specifically, for large spatial dimension N_s the maxima of the above quantities scale like

$$C_{\max} = C(\beta_{\max}) \sim N_s^{\alpha/\nu}, \quad (16)$$

$$\chi_{\max} = \chi(\beta_{\max}) \sim N_s^{\gamma/\nu}, \quad (17)$$

$$\chi_{\max}^\beta = \chi^\beta(\beta_{\max}) \sim N_s^{(1-\beta)/\nu}, \quad (18)$$

$$F_{\max}(\vec{k}) = F(\vec{k}; \beta_{\max}) \sim N_s^{2-\eta} \quad (19)$$

Definitions of the exponents α , β , γ , ν , η and *Finite Size Scaling* relations can be found in [15]. For a first order transition we have

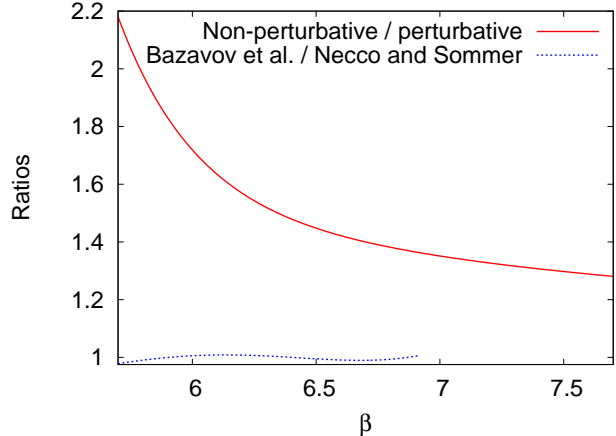


FIG. 1. SU(3) Λ_L : Non-perturbative corrections to the lambda lattice function $f_\lambda(\beta)$ and the ratio of two independent estimates of them.

$$\nu = \frac{1}{D}, \quad \frac{\alpha}{\nu} = D, \quad \frac{\gamma}{\nu} = D, \quad \frac{1-\beta}{\nu} = D, \quad (20)$$

where D is the dimension of the spatial volume of the system under study.

For η the situation of a first order transition is that one has a superposition of the disordered phase, where $\eta = 2$ holds, and the ordered phase with $\eta = 2 - D$ (at the critical point of a second order transition 2-point correlation fall off like $|\vec{r}|^{-D+2-\eta}$). This limits the usefulness of structure factors for equilibrium investigations of first order transitions, while they played some role in an investigation of the dynamics of the SU(3) deconfining transition [14]. As we have calculated $F(\vec{k})$ for the smallest momenta, $\vec{k} = (2\pi/N_s, 0, 0)$ and 90° rotations there off, we report maxima F_{\max} of this quantity together with maxima for our other observables.

B. SU(3) scaling

TABLE I. Effective Λ_L scales for fixed $T_t = 174$ MeV from pseudo-transition couplings $\beta_t(N_\tau)$ of the SU(3) deconfining phase transition.

N_τ	4	6	8	12
β_t	5.6925 (2)	5.8941 (5)	6.0625 (9)	6.3384 (13)
Λ_L (MeV)	5.0718 (23)	5.0731 (47)	5.0632 (74)	5.0262 (89)

Numerical evidence supports that SU(3) lattice gauge theory with the Wilson action (1) exhibits a weak first-order [16] deconfining phase transition at pseudo-transition coupling constant values $\beta_t(N_\tau) = 6/g_t^2(N_\tau)$. The *scaling behavior* of the deconfining temperature is

$$T_t = \frac{1}{a(\beta_t) N_\tau} = c_T \Lambda_L \quad (21)$$

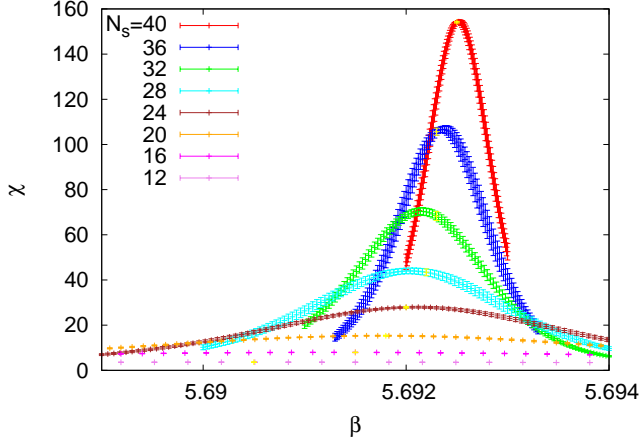


FIG. 2. Reweighted Polyakov loop magnetic susceptibilities for $N_\tau = 4$ PBC lattices.

where the lambda lattice scale ($g^2 = 6/\beta$)

$$a \Lambda_L = f_\lambda(\beta) = \lambda(g^2) (b_0 g^2)^{-b_1/(2b_0^2)} e^{-1/(2b_0 g^2)}, \quad (22)$$

has been *determined in the literature*. The coefficients b_0 and b_1 are perturbatively obtained [17] from the renormalization group equation,

$$b_0 = \frac{11}{3} \frac{3}{16\pi^2} \quad \text{and} \quad b_1 = \frac{34}{3} \left(\frac{3}{16\pi^2} \right)^2. \quad (23)$$

Using results from [10], higher perturbative and non-perturbative corrections are parametrized [14] by

$$\lambda(g^2) = 1 + e^{\ln a_1} e^{-a_2/g^2} + a_3 g^2 + a_4 g^4 \quad (24)$$

with $\ln a_1 = 18.08596$, $a_2 = 19.48099$, $a_3 = -0.03772473$ and $a_4 = 0.5089052$.

In the region of our MCMC simulations $\beta \in [5.7, 6.1]$ the non-perturbative correction is substantial as is visible from Fig. 1, where the ratio of the $f_\lambda(\beta)$ with and without ($\lambda(g^2) = 1$) the correction (24) is plotted. It is reassuring that our parametrization is well consistent with an independent earlier one [18] in the range of validity of the earlier parametrization for which the ratio of the two parametrizations is plotted in the lower part of Fig. 1 and the deviations from 1 are found to be less than 1%.

For PBC finite size corrections to the deconfining temperature T_t are negligible and we use the $N_\tau = 4, 6, 8, 12$ estimates of the transition coupling $\beta_t(N_\tau)$ from Ref. [10] to transform our scale $T_t = 174$ MeV into a value Λ_L . Using (3) and (21) we have

$$\Lambda_L = a^{-1} f_\lambda(\beta_t) = a^{-1} f_\lambda(\beta_t) a N_\tau T_t = \quad (25)$$

$$f_\lambda(\beta_t) N_\tau 174 \text{ MeV}. \quad (26)$$

Changing N_τ from 4 to 12, the variations of the resulting values of Λ_L are small as shown in Table I, which indicates that the SU(3) scaling limit is reached (the error

TABLE II. PBC: pseudo-transition temperatures and widths of the transition.

$N_\tau N_s^3$	β_t	T_t	L_s	$\Delta\beta_t^{4/5}$
4 12 ³	5.69055 (21)	173.193 (80)	3.412	0.01452 (17)
4 16 ³	5.69124 (16)	173.457 (61)	4.543	0.00666 (11)
4 20 ³	5.69175 (12)	173.652 (46)	5.672	0.003547 (73)
4 24 ³	5.69210 (14)	173.786 (54)	6.802	0.002015 (43)
4 28 ³	5.69226 (10)	173.847 (38)	7.932	0.001261 (20)
4 32 ³	5.69215 (07)	173.805 (27)	9.068	0.0008432 (96)
4 36 ³	5.69236 (07)	173.886 (27)	10.196	0.0005753 (70)
4 40 ³	5.69252 (05)	173.947 (20)	11.325	0.0004088 (26)
6 24 ³	5.89368 (34)	173.76 (11)	4.535	0.01091 (29)
6 30 ³	5.89346 (34)	173.69 (11)	5.671	0.00607 (19)
6 36 ³	5.89324 (27)	173.618 (87)	6.808	0.00384 (15)
6 42 ³	5.89387 (20)	173.820 (64)	7.934	0.00241 (11)
6 48 ³	5.89366 (20)	173.754 (64)	9.070	0.00167 (10)
6 54 ³	5.89400 (10)	173.862 (32)	10.198	0.001159 (31)
6 60 ³	5.89447 (09)	174.012 (30)	11.331	0.000821 (24)
8 32 ³	6.06144 (64)	173.94 (18)	4.530	0.01401 (61)
8 40 ³	6.06060 (53)	173.94 (18)	5.671	0.00791 (40)
8 48 ³	6.06207 (44)	174.11 (13)	6.789	0.00470 (28)
8 56 ³	6.06201 (37)	174.10 (11)	7.921	0.00307 (23)

bar for $N_\tau = 12$ is presumably underestimated). We turn this around to fix the infinite volume lambda lattice scale for this paper to

$$\Lambda_L = 5.07 \text{ MeV} \quad (27)$$

and calculate temperatures from

$$T = \frac{\Lambda_L}{N_\tau f_\lambda(\beta)} = \frac{5.07 \text{ MeV}}{N_\tau f_\lambda(\beta)}. \quad (28)$$

In the used natural units the lattice spacing is then expressed in fermi according to the equation

$$L_\tau = a N_\tau = (197.35 \text{ fermi}) \left(\frac{1 \text{ MeV}}{T} \right). \quad (29)$$

For $T = 174$ MeV we have $L_\tau = 1.13$ fermi.

C. Numerical results

In this section we report from our simulations with PBC. For $N_\tau = 4$ the reweighted [21] Polyakov loop susceptibilities are shown in Fig. 2 and corresponding estimates of pseudo-transition couplings β_t and temperatures T_t (in MeV) from all PBC lattices are compiled in Table II. Using (29) for $L_s = a N_s$ we give for the convenience of the reader also the spatial lattice size L_s in fermi.

The last column of Table II gives the full width at 4/5 maximum denoted by $\Delta\beta_t^{4/5}$. Due to the restricted range in which reweighting is possible one is forced to use

TABLE III. PBC: Maxima (values at β_{\max}) of observables.

$N_\tau N_s^3$	C_{\max}	χ_{\max}	χ_{\max}^β	F_{\max}
4 12 ³	0.3848 (21)	3.61 (03)	0.1680 (15)	0.648 (05)
4 16 ³	0.5333 (41)	7.96 (10)	0.3303 (38)	1.030 (07)
4 20 ³	0.7557 (79)	15.32 (20)	0.5885 (81)	1.490 (13)
4 24 ³	1.102 (15)	27.95 (44)	1.013 (16)	2.009 (20)
4 28 ³	1.555 (17)	45.84 (54)	1.592 (22)	2.482 (22)
4 32 ³	2.142 (22)	70.37 (59)	2.365 (23)	2.993 (21)
4 36 ³	2.989 (30)	106.69 (96)	3.497 (45)	3.479 (29)
4 40 ³	4.103 (22)	154.34 (73)	4.984 (19)	3.977 (15)
6 24 ³	0.1552 (07)	5.08 (10)	0.063 (02)	0.984 (37)
6 30 ³	0.1696 (10)	9.12 (21)	0.103 (03)	1.35 (11)
6 36 ³	0.1866 (19)	14.83 (43)	0.154 (05)	1.869 (29)
6 42 ³	0.2143 (31)	24.22 (78)	0.238 (08)	2.349 (51)
6 48 ³	0.2443 (48)	35.4 (1.6)	0.332 (15)	2.789 (74)
6 54 ³	0.2866 (34)	52.5 (1.0)	0.475 (09)	3.412 (43)
6 60 ³	0.3464 (57)	76.7 (1.6)	0.674 (16)	4.176 (50)
8 32 ³	0.10834 (28)	3.14 (09)	0.0196 (06)	0.677 (16)
8 40 ³	0.11080 (37)	5.57 (21)	0.0310 (11)	0.938 (20)
8 48 ³	0.11466 (55)	9.68 (41)	0.0498 (25)	1.269 (30)
8 56 ³	0.11988 (78)	15.62 (83)	0.0737 (35)	1.702 (85)

a height definition that is located unusually close to the maximum.

Other results, the maxima of the specific heat (11), of the magnetic (13) and thermal (14) Polyakov loop susceptibilities, and of structure factors (15) are collected in Table III. Their analysis is postponed to the section V.

IV. DECONFINING TRANSITION ON A DLT

In this section we report our DLT simulations. Our MCMC statistics per data point is the same as in the previous section for PBC.

A. Pseudo-transition temperatures

In Table IV we collect our estimates of pseudo-transition couplings β_t for $N_\tau = 4, 6$ and 8 . For each N_τ value three outside temperatures are used, which are approximately at the values given by Eq. (4). The precise values differ slightly, because the input to the computer program are rounded β_{out} values. Table IV gives these β_{out} values and in the rows below the resulting T_{out} in units of MeV using Eq. (27) for the conversion.

Due to the confined BC, the peaks of the Polyakov loop susceptibilities increase less pronounced with lattice size than for PBC (finite size scaling exponents are discussed in section V). Iteration towards inside coupling constant values β_{in} so that the pseudo-transition couplings β_t are included in their respective reweighting ranges can be quite tedious. Instead of relying on a single final simulation we often patched several together using the approach

TABLE IV. DLT pseudo-transition couplings.

N_τ	N_s	$\beta_{\text{out}} = 5.65$	$\beta_{\text{out}} = 5.66$	$\beta_{\text{out}} = 5.6767$
		$T_{\text{out}} = 158.09$	$T_{\text{out}} = 161.74$	$T_{\text{out}} = 167.95$
4	12	5.72266 (28)	5.71509 (40)	5.70265 (36)
4	16	5.72224 (16)	5.71589 (28)	5.70332 (32)
4	20	5.71962 (14)	5.71481 (14)	5.70392 (24)
4	24	5.71557 (22)	5.71249 (18)	5.70424 (20)
4	28	5.71225 (18)	5.710104 (95)	5.70379 (15)
4	32	5.708855 (68)	5.707564 (74)	5.70315 (12)
4	36	5.706273 (99)	5.705415 (74)	5.702297 (92)
4	40	5.704364 (80)	5.703607 (83)	5.701417 (83)
4	∞	5.692469 (42)	5.692469 (42)	5.692469 (42)
		$\beta_{\text{out}} = 5.84318$	$\beta_{\text{out}} = 5.85514$	$\beta_{\text{out}} = 5.87514$
		$T_{\text{out}} = 158.05$	$T_{\text{out}} = 161.70$	$T_{\text{out}} = 167.90$
6	24	5.93319 (35)	5.92418 (51)	5.90885 (64)
6	30	5.92846 (31)	5.92172 (25)	5.90937 (45)
6	36	5.92297 (31)	5.91905 (25)	5.90844 (21)
6	42	5.91816 (56)	5.91571 (26)	5.90777 (21)
6	48	5.91462 (26)	5.91289 (19)	5.90711 (24)
6	54	5.91136 (17)	5.91034 (13)	5.90622 (15)
6	60	5.90900 (13)	5.90802 (16)	5.90515 (20)
6	∞	5.89410 (11)	5.89410 (11)	5.89410 (11)
		$\beta_{\text{out}} = 6.004577$	$\beta_{\text{out}} = 6.018205$	$\beta_{\text{out}} = 6.040954$
		$T_{\text{out}} = 158.36$	$T_{\text{out}} = 162.01$	$T_{\text{out}} = 168.23$
8	32	6.10827 (61)	6.09684 (97)	6.08005 (53)
8	40	6.10099 (46)	6.09550 (41)	6.08086 (50)
8	48	6.09549 (48)	6.09210 (40)	6.07938 (34)
8	56	6.09071 (28)	6.08752 (32)	6.07841 (24)
8	64	6.08647 (25)	6.08403 (33)	6.07735 (29)
8	72	6.08322 (29)	6.08103 (36)	6.07590 (20)
8	∞	6.06212 (41)	6.06212 (41)	6.06212 (41)

of [22] for continuous variables. Fig. 3 and 4 show this for one of our CPU time expensive simulations of an $8 64^3$ DLT.

In Fig. 5 the β_t estimates for $N_\tau = 4, 6$ and 8 are plotted together (the connecting lines are just to guide the eyes). It is obvious that there are large separations by lattice size, whereas the split due to distinct outside temperatures is comparatively small (the larger β_t corresponding to the smaller β_{out} values). Applying the scaling relation (28) to translate our β_t into physical transition temperatures T_t we arrive at Fig. 6. The dominant separation is now by β_{out} values with different lattice sizes clustering due to scaling together. Scaling violations are visible, which increase towards small volumes. Assuming that for fixed outside temperature these violations die out according to (a lattice spacing, $x = N_\tau/N_s = L_\tau/L_s$ fixed)

$$\begin{aligned}
 aT(\infty; x) &= \frac{1}{N_\tau} + \frac{c_1(x)}{(N_\tau)^2} + \frac{c_2(x)}{(N_\tau)^3} + \dots \\
 &= aT(N_\tau; x) + \frac{c_1(x)}{(N_\tau)^2} + \frac{c_2(x)}{(N_\tau)^3} + \dots
 \end{aligned} \tag{30}$$

we extract $T(\infty; x)$ from fits

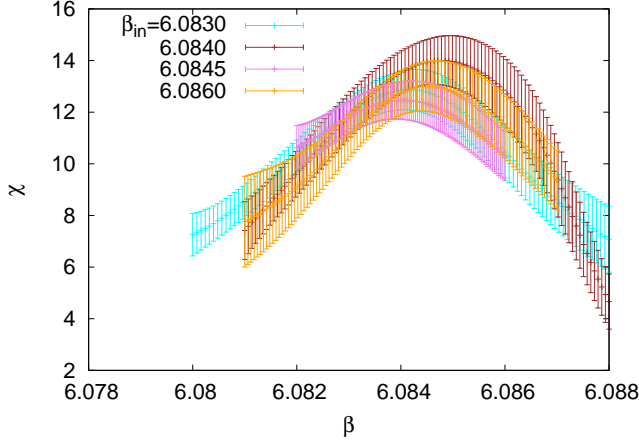


FIG. 3. Reweighting ranges of our final runs for the 864^3 DLT at $\beta_{\text{out}} = 6.018205$ ($T_{\text{out}} = 162$ MeV).

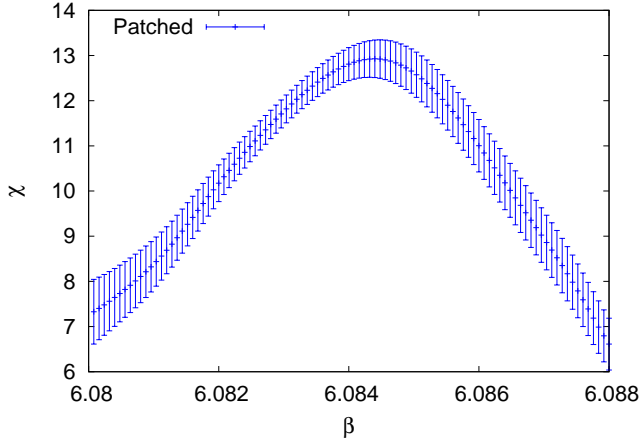


FIG. 4. Reweighting of the combined runs of the previous figure.

$$T(N_\tau; x) = T(\infty; x) + \frac{a_1(x)}{N_\tau}, \quad (31)$$

where $a_1(x) = c_1(x)T(N_\tau; x)$ carries the dimension of MeV. For each fit there are three data points $N_\tau = 4, 6$ and 8 with exception of $x = 0.1$ for which we have only $N_\tau = 4$ and 6 . The results for $T(\infty; x)$ are collected in Table V together with each goodness of fit Q . Small Q values indicate that the data are sensitive to higher order correction to Eq. (31), which we cannot handle with only three N_τ values. Visual inspection of the fits show even in the (due to rounding) $Q = 0$ cases a monotonous arrangement of the data points in agreement with the slopes of the fit curves.

Our estimates of $T(\infty; x)$ are plotted in Fig. 7 together with fits of the form

$$T(\infty; x) = T(\infty, 0) + a_1 x. \quad (32)$$

As surface over volume varies $\sim x$, it is natural to assume that the small volume corrections of an effective transition temperature are of this form. For comparison

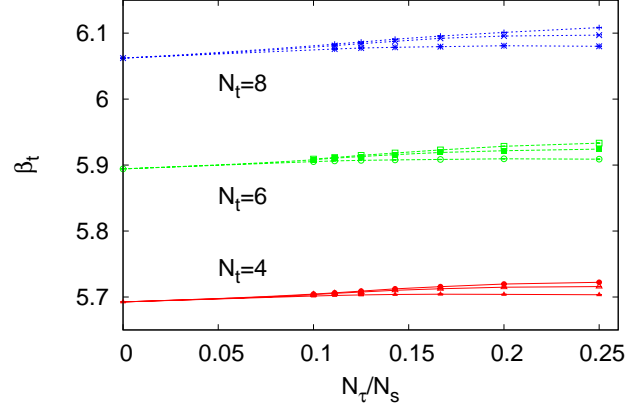


FIG. 5. All pseudo-transition estimates β_t .

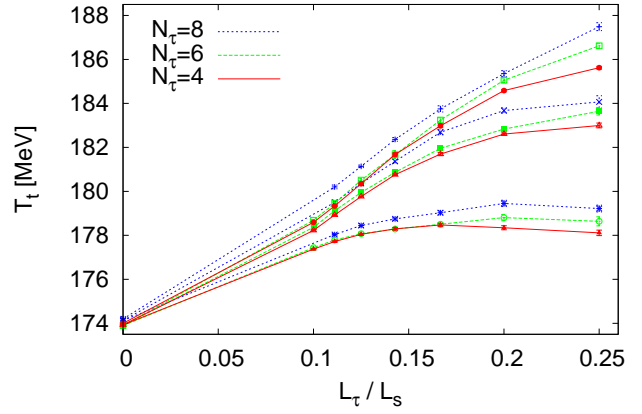


FIG. 6. All pseudo-transition temperature T_t estimates.

we have also added $T(\infty, x)$ estimates from lattices with PBC, which give the essentially flat line at the bottom of the figure. For the three outside temperatures we find the fit parameters

$$a_1 = 61.13 (77) \text{ MeV for } T_1 (Q = 0.20), \quad (33)$$

$$a_1 = 54.17 (93) \text{ MeV for } T_2 (Q = 0.11), \quad (34)$$

$$a_1 = 36.92 (98) \text{ MeV for } T_3 (Q = 0.11) \quad (35)$$

and with PBC a value that is consistent with zero

$$a_1 = 0.35 (76) \text{ MeV } (Q = 0.19). \quad (36)$$

Some data were not included in the fits: For outside temperatures T_1 and T_2 the $x = 0.1$ estimates for T_t , because at $x = 0.1$ a $N_\tau = 8$ lattice was too large to simulate and the T_t estimate from just $N_\tau = 4$ and 6 is deemed to be unreliable. Furthermore, T_t estimates from large x are omitted once they leave the straight line. Their turnaround contradicts the expectation that the influence of the confined outside increases in proportion to the surface over volume ratio. It is assumed to be an artifact

TABLE V. To $N_\tau = \infty$ extrapolated pseudo-transition temperatures in MeV with $x = N_\tau/N_s$.

x	T_1		T_2		T_3	
	T_t	Q	T_t	Q	T_t	Q
0	173.92 (10)	0.05	173.92 (10)	0.05	173.92 (10)	0.05
1/10	179.02 (15)	—	178.66 (17)	—	177.58 (21)	—
1/9	180.46 (14)	0.00	179.68 (12)	0.02	178.21 (11)	0.03
1/8	181.66 (13)	0.00	180.64 (14)	0.02	178.63 (15)	0.01
1/7	182.90 (18)	0.04	181.69 (16)	0.01	178.98 (14)	0.00
1/6	184.24 (24)	0.22	183.20 (20)	0.00	179.21 (18)	0.00
1/5	186.09 (22)	0.82	184.10 (19)	0.00	180.34 (27)	0.12
1/4	189.03 (27)	0.31	185.03 (42)	0.79	180.22 (31)	0.37

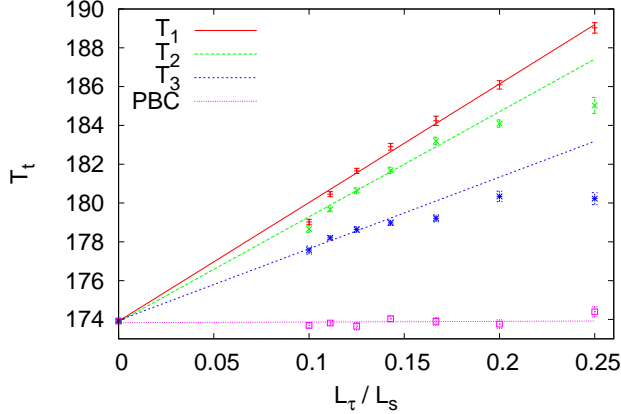


FIG. 7. Estimated behavior of pseudo-transition temperature for decreasing volume.

due to our choice of the DLT for implementing the confined outside. As outlined in [3], one can wind around each DLT layer along the diagonals. This leads to corner effects, where the inside phase connects with itself. Their importance appears to increase for smaller volumes and with decreasing temperature of the outside layer. The finally used numbers of data were 7 for T_1 , 5 for T_2 and 5 for T_3 as can be deduced from figure 7 (for PBC all data points are used).

B. Width

In Table VI we report our estimates of $\Delta\beta_t^{4/5}$, as in section III C the full width at 4/5 of the maximum of the Polyakov loop susceptibility. After converting these values into physical units to $\Delta T_t^{4/5}$, there are rather large scaling violation from $N_\tau = 4$ to $N_\tau = 6$, while the situation improves considerably from $N_\tau = 6$ to $N_\tau = 8$. For outside temperature T_3 this is illustrated in Fig. 8 (to guide the eyes data points are connected by straight lines).

We combine the widths similarly as before the pseudo-

TABLE VI. Widths $\Delta\beta_t^{4/5}$ of the magnetic Polyakov loop susceptibilities.

N_τ	N_s	$\beta_{\text{out}} = 5.65$	$\beta_{\text{out}} = 5.66$	$\beta_{\text{out}} = 5.6767$
		4	12	0.01767 (19)
4	16	0.00890 (11)	0.00805 (15)	0.00713 (15)
4	20	0.00539 (10)	0.00472 (08)	0.00379 (10)
4	24	0.00422 (16)	0.00323 (11)	0.002276 (56)
4	28	0.00335 (14)	0.002531 (78)	0.001498 (44)
4	32	0.002580 (71)	0.002185 (65)	0.001089 (44)
4	36	0.001986 (85)	0.001688 (64)	0.000869 (40)
4	40	0.001574 (69)	0.001319 (58)	0.000718 (38)
		$\beta_{\text{out}} = 5.84318$	$\beta_{\text{out}} = 5.85514$	$\beta_{\text{out}} = 5.87514$
6	24	0.01458 (30)	0.01365 (42)	0.01191 (35)
6	30	0.00919 (26)	0.00837 (21)	0.00676 (24)
6	36	0.00674 (28)	0.00563 (19)	0.00419 (13)
6	42	0.00516 (23)	0.00462 (26)	0.00289 (11)
6	48	0.00402 (28)	0.00350 (16)	0.00197 (11)
6	54	0.00320 (17)	0.00278 (13)	0.00159 (14)
6	60	0.00250 (13)	0.00224 (15)	0.00131 (10)
		$\beta_{\text{out}} = 6.004577$	$\beta_{\text{out}} = 6.018205$	$\beta_{\text{out}} = 6.040954$
8	32	0.01780 (43)	-	0.01471 (36)
8	40	0.01175 (39)	0.01008 (35)	0.00824 (32)
8	48	0.00882 (56)	0.00658 (47)	0.00540 (22)
8	56	0.00629 (58)	0.00484 (24)	0.00359 (13)
8	64	-	0.00422 (21)	0.00245 (17)
8	72	0.00365 (21)	0.00343 (39)	0.00202 (17)

transition temperatures by Eq. (31) and give the results in Table VII, where x stands for the limit

$$x = N_\tau/N_s = \text{constant}, \quad N_\tau \rightarrow \infty. \quad (37)$$

Compared to the pseudo-transition temperatures in Table V the goodness of the fits is greatly improved, but this has mainly to be attributed to the much larger relative errors of the widths. When there were only $N_\tau = 4$ and 6 data points, there is no goodness of fit as well as at $x = 0$, where the transition becomes sharp, so that the width is known to be zero.

In Fig. 9 the $N_\tau = \infty$ width estimates are plotted for the three outside temperatures T_1 , T_2 and T_3 together with the similarly combined estimates from our simulations with PBC. For a first order phase transition the peaks of the Polyakov loop susceptibility develop δ -function like singularities, i.e., with the maximum increasing proportional to the spatial volume. Therefore, their widths decrease in leading order proportional to x^3 . However, fitting

$$\Delta T_t^{4/5} = a_1 x^3 \quad (38)$$

acceptable goodness of fit values are only obtained by restricting the fits to the smallest x values, which are obtained from the largest $(N_s)^3$ volumes simulated for $N_\tau = 4, 6$ or 8. These fits are also drawn in Fig. 9. The numbers of data points included are: 4 for T_1 and T_2 , 5

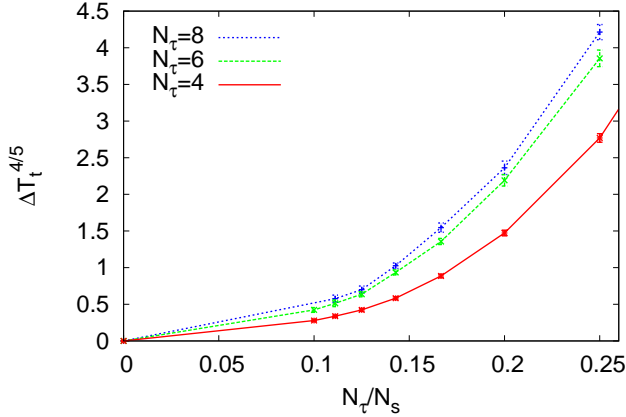


FIG. 8. Widths estimates for outside temperature T_3 and temporal lattice sizes $N_\tau = 4, 6, 8$.

TABLE VII. To $N_\tau = \infty$ extrapolated widths in MeV with $x = N_\tau/N_s$. Power law fit parameters in the last row.

x	T_1		T_2		T_3	
	$\Delta T_t^{4/5}$	Q	$\Delta T_t^{4/5}$	Q	$\Delta T_t^{4/5}$	Q
0	0.0 (0)	—	0.0 (0)	—	0.0 (0)	—
1/10	1.21 (14)	—	1.15 (16)	—	0.71 (11)	—
1/9	1.40 (11)	0.24	1.37 (12)	0.75	0.83 (09)	0.76
1/8	1.91 (29)	—	1.61 (11)	0.50	1.01 (08)	0.55
1/7	2.39 (21)	0.80	1.96 (13)	0.01	1.52 (07)	0.20
1/6	3.38 (24)	0.73	2.84 (17)	0.18	2.25 (10)	0.61
1/5	4.77 (19)	0.77	4.25 (16)	0.08	3.37 (16)	0.21
1/4	7.14 (21)	0.20	7.12 (43)	—	5.75 (20)	0.36
—	a_2	Q	a_2	Q	a_2	Q
—	1.962 (72)	0.97	2.080 (92)	0.66	2.393 (71)	0.91

for T_3 and 5 for PBC. To understand the effect better, we performed two-parameter fits to the form

$$\Delta T_t^{4/5} = a_1 x^{a_2}, \quad (39)$$

which leave the exponent variable. Surprisingly, this allows us to fit all our widths data consistently as shown in Fig. 10. Together with the goodness of fit the estimated exponents are given in the last row of Table VII. The pattern is that disorder (decreasing outside temperature) reduces the thus obtained a_2 exponents, so that they look effectively like exponents expected for second order phase transitions. Apparently much larger lattices and smaller error bars (increased statistics) are needed to exhibit the weak first order nature of the transition. This is even true for PBC, though the obtained effective exponent is the largest: $a_2 = 2.620$ (57) with $Q = 0.75$.

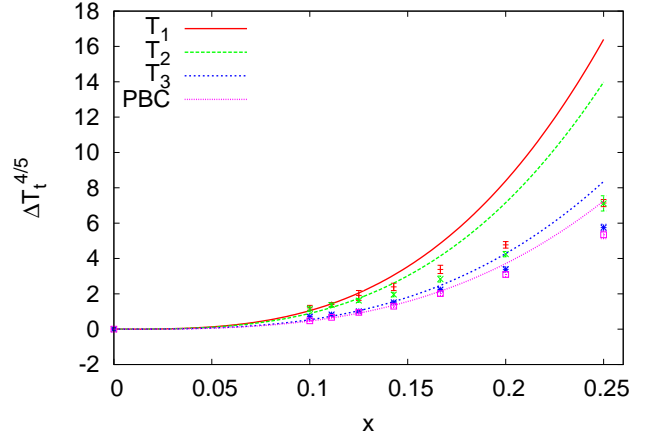


FIG. 9. Widths estimates for $N_\tau = \infty$ and outside temperatures T_1, T_2, T_3 . The lines are x^3 fits to the widths at the smallest x .

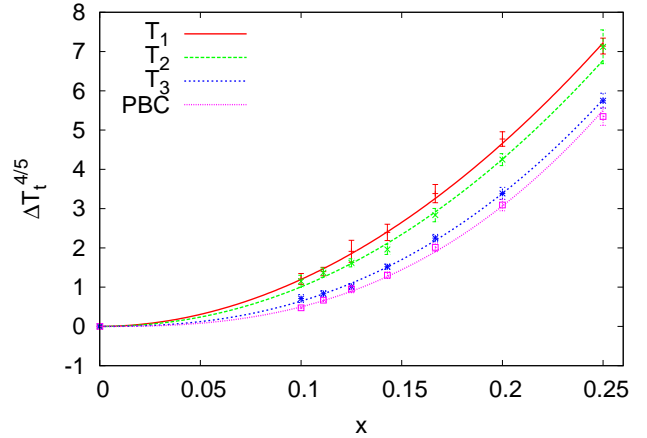


FIG. 10. Widths estimates for $N_\tau = \infty$ and outside temperatures T_1, T_2, T_3 . The lines are two-parameter fits (39) to the widths.

V. FINITE SIZE SCALING EXPONENTS

Here we consider the influence of DLT BCs with different outside temperatures on the finite size scaling exponents of the specific heat C , the magnetic Polyakov loop susceptibility χ and the thermal Polyakov loop susceptibility χ^b . We extract estimates from the finite size behavior of their maxima C_{\max} , χ_{\max} and χ_{\max}^b by performing two-parameter fits

$$Y(N_s) = a(N_s)^b. \quad (40)$$

Smaller lattices are omitted until an acceptable goodness of fit Q is obtained.

For fixed N_τ and $N_s \rightarrow \infty$ one has to obtain the same exponents as with PBC, because we are still dealing with

TABLE VIII. Estimates of finite size scaling exponents from two-parameter fits (40) for our data with DLT BC and PBC.

	C_{\max}			χ_{\max}			χ_{\max}^b		
	b	Q	n	b	Q	n	b	Q	n
	$N_\tau = 4$			$N_\tau = 4$			$N_\tau = 4$		
T_1	0.776 (80)	0.97	4	1.381 (36)	0.33	6	1.163 (70)	0.30	5
T_2	0.83 (15)	0.73	3	1.75 (18)	0.73	3	1.52 (26)	0.67	3
T_3	1.27 (11)	0.24	4	2.01 (11)	0.29	4	1.70 (13)	0.26	4
PBC	2.925 (51)	0.39	3	3.441 (30)	0.16	4	3.343 (46)	0.86	3
	$N_\tau = 6$			$N_\tau = 6$			$N_\tau = 6$		
T_1	0.242 (09)	0.83	7	1.569 (55)	0.91	6	1.198 (58)	0.91	6
T_2	0.275 (09)	0.57	7	1.702 (48)	0.05	6	1.323 (49)	0.10	6
T_3	0.591 (21)	0.86	6	2.219 (83)	0.20	5	2.173 (40)	0.13	7
PBC	1.58 (12)	0.16	3	3.195 (64)	0.36	5	2.863 (70)	0.31	5
	$N_\tau = 8$			$N_\tau = 8$			$N_\tau = 8$		
T_1	0.0898 (38)	0.26	6	1.537 (77)	0.12	5	1.220 (55)	0.11	6
T_2	0.1074 (55)	0.39	6	1.637 (95)	0.69	5	1.279 (77)	0.18	5
T_3	0.1956 (94)	0.20	5	2.637 (70)	0.51	6	2.215 (47)	0.69	6
PBC	0.222 (20)	0.17	3	2.824 (92)	0.36	4	2.345 (93)	0.29	4

a weak first order phase transition and the asymptotic behavior does not depend on the BC. However, effective estimates from our actually used lattices show strong deviations from the asymptotic behavior. They are compiled in Table VIII. Instead of the predicted (20) first order exponent $b = D = 3$ far smaller values are obtained. With N_τ fixed the systematic trend is that the exponents for outside temperature T_3 are larger than those for T_1 and T_2 . To give an example, we show in Fig. 11 the fits of the maxima of the magnetic susceptibility for $N_\tau = 6$ lattices.

For χ_{\max} the used data are compiled in Table IX and the other maxima can be found in [19]. One may assume that larger N_τ values need also larger spatial lattice sizes N_s to exhibit asymptotic behavior. Our data take care of this by keeping $x = N_s/N_\tau$ for all N_τ in the same range. Nevertheless the scaling behavior of the specific heat is for $N_\tau = 8$ in all cases, including PBC, erratic. Surprisingly, the $C(\beta)$ curves show only a very broad peaks. They are expected to sharpen for even larger N_s , but those were out of our computational means.

VI. SUMMARY AND CONCLUSIONS

Our simulations show that even for relatively small temperature differences between outside and inside volumes sizeable small volume corrections survive for pseudo-transition temperatures. For a L_s^3 box with edge length L_s between 4 and 12 fermi Fig. 12 show the volume dependence of our present estimates from PBC and DLT calculations together with those with CBC from Ref. [2]. With PBC there are practically no finite size corrections. Then, pseudo-transition temperatures increase when the outside temperature falls below the infinite volume de-

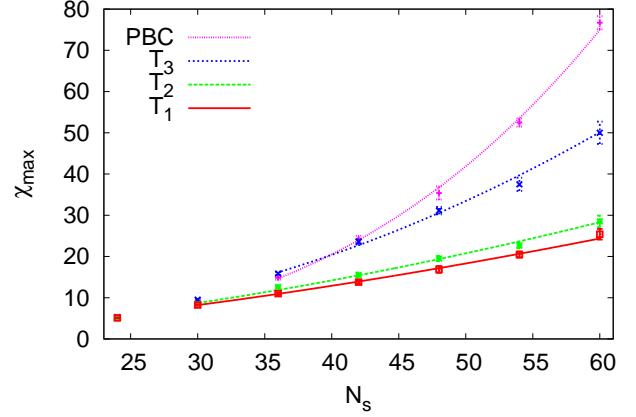


FIG. 11. Two-parameter exponent fits for the magnetic susceptibility χ_{\max} on $N_\tau = 6$ lattices.

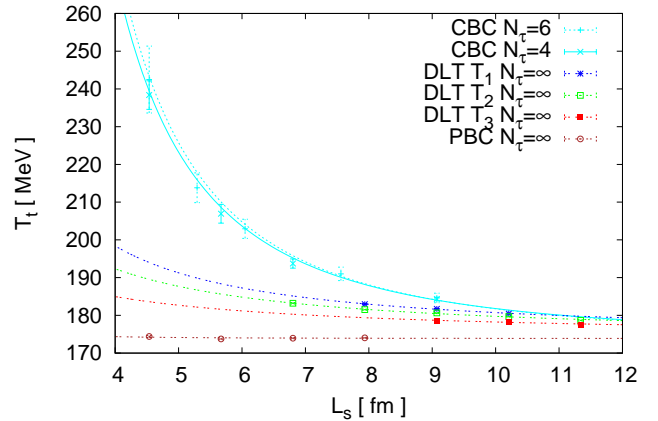


FIG. 12. Small volume corrections for the pseudo-transition temperature with CBC, DLT and PBC boundaries.

confining transition temperature, which is here set to 174 MeV. For the outside temperatures (4) used in this paper the change is less pronounced than with CBC, but astonishingly large when one bears in mind that CBC are supposed to model zero outside temperature. This supports that CBC estimates are realistic and not just a strong coupling artifact.

While a lot of work has focused on including quarks, little has so far been done about calculating small volume corrections, which increase the SU(3) transition temperature, while quark effects decrease it. The SU(3) simulations suggest that the magnitudes of the changes are similar. Assuming that the increase with decreasing volume holds also with quarks included, lattice calculations with PBC underestimate the pseudo-transition temperature in RHIC. The width of the transition is broadened by both effects, so that the conversion into a cross-over is expected to become even more pronounced. See Fig. 10

TABLE IX. DLT: Maxima χ_{\max} of the Polyakov loop susceptibility (values at β_{\max}).

N_τ	N_s	$\beta_{\text{out}} = 5.65$	$\beta_{\text{out}} = 5.66$	$\beta_{\text{out}} = 5.6767$
4	12	3.67 (03)	3.75 (04)	3.63 (04)
4	16	7.58 (07)	8.01 (11)	8.27 (13)
4	20	12.56 (17)	13.90 (17)	16.20 (30)
4	24	15.81 (41)	20.25 (49)	27.89 (50)
4	28	19.09 (54)	25.47 (57)	42.80 (92)
4	32	23.54 (46)	28.31 (61)	58.9 (1.8)
4	36	28.42 (86)	34.49 (93)	72.4 (2.4)
4	40	33.8 (1.1)	42.1 (1.5)	86.4 (3.3)
		$\beta_{\text{out}} = 5.84318$	$\beta_{\text{out}} = 5.85514$	$\beta_{\text{out}} = 5.87514$
6	24	5.11 (08)	5.04 (11)	5.30 (11)
6	30	8.23 (17)	8.51 (15)	9.53 (24)
6	36	11.00 (34)	12.60 (30)	15.86 (35)
6	42	13.77 (43)	15.51 (60)	23.58 (64)
6	48	16.86 (83)	19.52 (63)	31.12 (90)
6	54	20.47 (75)	22.68 (73)	37.5 (1.6)
6	60	25.4 (1.3)	28.5 (1.4)	50.0 (2.7)
		$\beta_{\text{out}} = 6.004577$	$\beta_{\text{out}} = 6.018205$	$\beta_{\text{out}} = 6.040954$
8	32	3.556 (69)	3.27 (11)	3.35 (12)
8	40	5.39 (13)	5.98 (13)	6.43 (17)
8	48	7.14 (24)	8.46 (39)	10.27 (31)
8	56	9.30 (31)	10.48 (68)	14.98 (87)
8	64	9.41 (71)	12.46 (74)	21.7 (1.2)
8	72	13.65 (63)	16.1 (1.3)	27.5 (2.1)

for the width estimates of this paper.

To include quarks in such calculations requires to build on software of one of the large scale QCD collaborations. At least in a first stage one should fall back to simple CBC as one cannot afford a multiplicative CPU time increase due more involved BCs and to fermions. The limitation appears acceptable, as our SU(3) DLT calculations support the relevance of the earlier CBC estimates. Already for CBC modifications of, e.g., the MILC code would be laborious, because to reduce discretization errors one has implement CBC for improved actions like [23] in both gauge and fermionic sectors.

A supporting investigation could aim at a further perfection of the BC between cold and hot regions of pure SU(3) gauge theory. This should include to study the effect due to a cold surrounding geometry instead of a DLT. Using the always confined [24] spacelike string tension as an additional scale would allow one to tune couplings for spacelike and timelike plaquettes distinctly, so that the spacelike transition from deconfined to confined volumes becomes entirely smooth.

ACKNOWLEDGMENTS

This work was in part supported by the US Department of Energy under contracts DE-FA02-97ER41022 and DE-FG02-13ER41942. In addition, we received generous CPU time support from the National En-

ergy Research Scientific Computing Center (NERSC) and our data were generated under NERSC Energy Research Computing Allocations Process (ERCAP) requests 84866, 84861, 84795, 84105, 85832 and 85833.

-
- [1] C. Spieles, H. Stocker and C. Greiner, Phys. Rev. C **57**, 908 (1998); A. Gopie and M.C. Ogilvie, Phys. Rev. D **59**, 034009 (1999); L.M. Abreu, M. Gomes and A.J. da Silva, Phys. Lett. B **642**, 551 (2006);
 - [2] A. Bazavov and B.A. Berg, Phys. Rev. D **76**, 014502 (2007).
 - [3] B.A. Berg, A. Bazavov and Hao Wu, POS (Lattice 2009) 164.
 - [4] N. Yamamoto and T. Kanazawa, Phys. Rev. Lett. **103**, 032001 (2009).
 - [5] L.F. Palhares, E.S. Fraga and T. Kodama, J. Phys. G **37**, 094031 (2010); **38**, 085101 (2011); E.S. Fraga, L.F. Palhares and P. Sorensen, Phys. Rev. C **84**, 011903(R) (2011).
 - [6] J. Braun, B. Klein, H.J. Pirner and A.H. Rezaeian, Phys. Rev. D **73**, 074010 (2006); J. Braun, B. Klein and B.-J. Schaefer, Phys. Lett. B **713**, 216 (2012).
 - [7] A. Bhattacharyya, P. Deb, S.K. Ghosh, R. Ray and S. Sur, Phys. Rev. D **87**, 054009 (2013).
 - [8] K.G. Wilson, Phys. Rev. D **10**, 2445 (1974).
 - [9] L. Levkova, POS (Lattice 2011) 011.
 - [10] G. Boyd, J. Engels, F. Karsch, E. Laermann, C. Legeland, M. Lütgemeier and B. Peterson, Nucl. Phys. B **469**, 419 (1996).
 - [11] B.A. Berg and Hao Wu, Comp. Phys. Commun. **183**, 2145 (2012).
 - [12] H.J. Rothe, *Lattice Gauge Theories: An Introduction*, 3rd edition, World Scientific, Singapore 2005.
 - [13] H.E. Stanley, *Introduction to Phase Transitions and Critical Phenomena*, Clarendon Press, Oxford, 1971, pp. 98.
 - [14] A. Bazavov, B.A. Berg and A. Velytsky, Phys. Rev. D **74**, 014501 (2006).
 - [15] A. Pelissetto and E. Vicari, Phys. Rep. **368**, 549 (2002) [cond-mat/0012164].
 - [16] M. Fukugita, M. Okawa and A. Ukawa, Nucl. Phys. B **337**, 181 (1990) and references given therein.
 - [17] D.J. Gross and F. Wilczek, Phys. Rev. Lett. **30**, 1343 (1973); H.D. Politzer, Phys. Rev. Lett. **30**, 1349 (1973).
 - [18] S. Necco and R. Sommer, Nucl. Phys. B **622**, 328 (2002).
 - [19] H. Wu, Dissertation, Florida State University, Physics Department (2012).
 - [20] G. Parisi, R. Petronzio and F. Rapuano, Phys. Lett. B **128**, 418 (1983).
 - [21] A.M. Ferrenberg and R.H. Swendsen, Phys. Rev. Lett. **61**, 1195 (1988); **63**, 1658 (1989) and references given therein.
 - [22] N.A. Alves, B.A. Berg and S. Sanielevici, Nucl. Phys. B **376**, 218 (1992).
 - [23] A. Bazavov et al., Rev. Mod. Phys. **82**, 1349-1417 (2010); A. Bazavov and P. Petreczky, J. Phys. G **34**, 124099

(2011) [arXiv:1107.5027].

- [24] O. Andreev, Phys. Lett. B **659**, 416-420 (2008)
[arXiv:0709.4395] and references given therein.